Multifunctional material design for strain sensing: carbon black effect on mechanical and electrical properties of polyamides

Multifunctional material design for strain sensing: carbon black effect on mechanical and electrical properties of polyamides

Alberto Ciampaglia[a,*], Raffaele Ciardiello[a], Federico Cesano[b], Giovanni Belingardi[a], Valentina Brunella[b]

[a]*Department of Mechanical and Aerospace Engineering, Politecnico di Torino, Turin, Italy*

[b]*Department of Chemistry, Università di Torino, Turin, Italy*

**Corresponding author*

Email address: alberto.ciampaglia@polito.it (A. Ciampaglia)

Keywords: *PMC, polymers, PA6, smart material, nanoparticles, conductivity*

Abstract

This work investigates the coupled effect on the mechanical and electrical properties of carbon black (CB) dispersed in polyamide 6,6 matrix. The amount of CB added to the polymer matrix was varied between c.a. 5 and c.a. 25 wt %. The presented results reveal the capability of conductive carbon nanostructured particles, known as carbon black, to functionalize the thermoplastic polymers by activating conductive percolation networks, as obtained over the percolation threshold. The electrical resistivity of the composite compounds under static and dynamic conditions was determined. In this domain, the

variation of the electrical properties with the applied stress, is assessed through mechanical tests with in-situ electrical measurements. The conductivity sensitivity of reinforced composites to the applied strain is analyzed within direct (DC) and alternate current (AC) regime, revealing the effect of frequency on the composite strain sensitivity. An investigation on the morphology of particle dispersion at the microscopic level highlights the role played by microstructural arrangements on the homogenized bulk properties of composites. Mean field homogenization models for the estimation of composite stiffness are compared to the experimental results.

1 Introduction

Polymeric matrix composite (PMC) materials are gaining high interest in the industry and scientific community: their unique properties have paved the way to their usage for numerous applications. However, polymers are insulating, meaning that cannot conduct current. During the last decade, researchers have proved the capability of carbon nanoparticles of modifying the properties of PMC even at the macro-scale. In this regard, great accomplishment can be found in several characteristics, including stiffness enhancement(1–4), strength increase(5), induced plasticity(6), toughening mechanism(7,8), electrical conductivity(9–11), strain sensing (12–23). The evolution of the micro-mechanic alongside with material science knowledge has opened the doors to a boundless portfolio of materials, which properties can be tailored on the design specification by properly defining material constituents and architecture from the nano to the micro scale. The spread of these “smart materials” has not dispensed industrial sectors such as aerospace(24) or automotive(25,26), where functional material can help

designers cutting costs, producing lighter structures, and adding new functionalities as structural health monitoring(27–30) (SHM). SHM is an inverse technique aiming at assessing the health state of a structure by processing signals from sensors mounted on the monitored part. The adoption of innovative materials (fiber-reinforced composites, sandwich structures, multi-material laminates), for which the study on fatigue response and damage tolerant design have not been consolidated yet, put the requirement for a reliable, but affordable and lightweight SHM. In accomplishing this, smart self-sensing materials are ideal candidates. Indeed, self-sensing materials shows a change in the electrical conductivity when a stress (or strain) is applied; this phenomenon is usually activated by highly conductive particles (e.g., carbon nanotube, carbon fibers) dispersed into the polymer(31).

The adoption of such materials in SHM allows monitoring large structures without any sensor: every point of the smart material structure is monitorable and the cost increase only relies on the functionalizing particle addition to the neat polymer. The goal of this work is to comprehensively study the effect of Carbon Black (CB) particles loading on the mechanical, electrical and strain sensing properties of polyamide 6 and polyamide 66 (PA6 and PA66, respectively). First, we manufactured CB-PA composites with injection molding as described in Section 2.1. In Section 2.2 particles concentration and morphology are analyzed with Scanned Electron Microscopy (SEM) and Thermogravimetric Analysis (TGA), while the percolation threshold of CB reinforced PA is established; in Section 3.1, the effect of particles concentration on the stiffness and strength of composites is experimentally investigated through tensile tests and correlated with different homogenization models. In Section 3.3, we present the results of tensile

tests with in-situ resistance and impedance measurements on conductive and propose a novel model for the estimation of the material Gauge Factor (GF) variation with the applied electric frequency. At the best of authors knowledge, this work is the first revealing the effect of the excitation current frequency on the self-sensing material gauge factor.

2 Materials and methods

2.1 Materials

Composite specimens were manufactured starting from commercial PA6/CB masterbatch (Cabelec CA3178, polyamide 6 with 27,5 wt.% of CB, MFI= 10 g/10 min at 275°C) with addition of PA6 (polyamide 6 TECHNYL C 206, Solvay) or PA66 (polyamide 66 TECHNYL A 205F, Solvay). Polymers and the compound were melt-compounded by using a Babyplast 6/10P micro injection molding machine (Rambaldi srl, Italy) having a type-V tensile test specimen mold (ASTM D638). Prior to use, the polymers and masterbatch were dried at 80°C for 4 h, while barrel, injection, nozzle, and mold temperatures were set at 255, 250, 245, and 60°C for PA6, or 280, 275, 270 and 70°C for PA66 compositions, respectively.

2.2 Experimental tests

2.2.1 *TGA*

Thermogravimetric measurements were performed with a TA Q500 instrument, TA Instruments, by using c.a. 8-10 mg of sample. The temperature was increased from 50 °C to 700 °C under nitrogen (N_2) gas flow, then to 800 °C in air (heating rate: 10 °C/min in both steps). This method was adopted to determine the polymer and CB contents after compounding.

2.2.2 *SEM*

Field-emission Scanning Electron Microscopy (FeSEM), Tescan Mira 3 (Tescan, Brno, Czech Republic) was used to assess the particle distribution of the specimens and the corresponding fracture surfaces. An accelerating voltage of 5 kV was used together with a secondary emission signal. The specimen surfaces were not coated with metals since the specimens were electrically conductive and to avoid possible contaminations.

2.2.3 *DC electrical properties*

DC electrical properties were obtained under static conditions by using a conventional two-point probe technique with the specimen connected with a Keithley 2420 source meter. Compounds were cut to obtain smaller specimens c.a. 20 × 14 × 2 mm in size. Both faces of specimens were polished to eliminate the outermost surface and Ag conductive paste was used to make round shaped electrodes with an average diameter of 2mm. Electrical resistivity (ρ) was obtained by using the equation: $\rho = R \times (A/d)$, where R is the measured resistance, A is the sample cross-section, and d is the distance between

electrodes. Hence, obtained values were referred to as volume resistivity. Measurements were obtained by placing the specimens in a homemade sample holder consisting of a fixed side and a spring-loaded electrode.

2.2.4 Tensile test with in-situ conductivity measure

The tensile tests have been conducted with the universal test machine Zwick/Roell Z5.0 with a maximum load of 5kN in the displacement control mode with a crosshead rate of 5 mm/min. The strain is then computed as the ratio of the crosshead displacement over the initial grip distance.

To measure the in-situ electrical response, the Hioki 3538 impedance meter is connected to the silver epoxy electrodes on the specimen's surface through a 4-point probe connector. Four-terminal sensing is an electrical impedance measuring technique using separate pairs of current and voltage sensing electrodes, eliminating the contact resistance from the measurements. The electrical frequency response in the range of 0-10 kHz is measured at each displacement increment of 50 μm, while keeping the crosshead position fixed. The dynamic range is sampled within evenly logarithmic spaced frequency intervals. Due to the visco-elasto-plastic nature of the polymer, a stress relaxation can be observed while the strain is fixed, resulting in a decrease of the measured force during the measurement window. The effect has been attenuated by applying a low displacement rate of 5mm/min.

2.3 Homogenization models

2.3.1 Voigt model

Due to the heterogeneous nature of the composites under study, the effect of CB loading in the polyamide matrix can be analyzed by mean-field homogenization theories. Under the assumptions of constant strain in the Representative Volume Element (RVE), negligible interaction between inclusions and homogeneously dispersed particles - the Voigt model(32) can estimate the composite elastic modulus E_c from the volume fraction of particles:

$$E_c = Em \cdot v_m + E_p \cdot v_p$$

Where E_m and E_p are the Young's Modulus of the matrix and the particles respectively, and v_m and v_p the volume fractions. Since the particle content has only been measured as weight percentage, the volume fraction is computed by means of the density ratio between matrix and inclusions. The density of PA6, PA66 and Carbon Black(4) are assumed to be 1.1, 1.1 and 1.8 g/cm^3, respectively.

2.3.2 Strain gradient elasticity theories

The classical estimates (bounds) of the Hashin-Shtrikman type for materials with an isotropic distribution of the phases(33) read:

$$\underline{\mu} = \mu^{(1)} + \frac{c_2(\mu^{(2)}-\mu^{(1)})}{1+c_1\frac{\mu^{(2)}-\mu^{(1)}}{\mu^*+\mu^{(1)}}} \quad \text{and} \quad \underline{k} = k^{(1)} + \frac{c_2(k^{(2)}-k^{(1)})}{1+c_1\frac{k^{(2)}-k^{(1)}}{k^*+k^{(1)}}} \tag{3}$$

150

151 with μ^* and k^* the shear and bulk moduli of the Hill constraint tensor:

152

153 $$\mu^* = \frac{\mu^0(9k^0+\mu^0)}{6(k^0+2\mu^0)} \quad \text{and} \quad k^* = \frac{4}{3}\mu^0 \tag{4}$$

154

155 The choice $\mu^0 = \mu^{(1)}$ *and* $k^0 = k^{(1)}$ corresponds to the lower Hashin-Shtrikman bound
156 which coincides with the Mori Tanaka (MT) model (34) while the choice $\mu^0 = \mu^*$ and
157 $k^0 = k^*$ defines the self-consistent (SC) estimate (35).

158 Homogenization methods utilizing classical elasticity-based Eshelby tensors cannot
159 capture the particle size effect experimentally observed in particle–matrix composites at
160 the micron and nanometer scales. A simplified strain gradient elasticity theory (SSGET)
161 for spherical inclusion has been proposed by Gao and Ma(36), that introduced one
162 material length scale parameter instead of two classical elastic constants.

163 Equation 4 is rearranged as follows:

164

165 $$\underline{k} = k^{(1)} + k^{(1)}\frac{c_2(k^{(2)}-k^{(1)})}{k^{(1)}+c_1(k^{(2)}-k^{(1)})S_p} \quad \text{and} \quad \underline{\mu} = \mu^{(1)} + \mu^{(1)}\frac{c_2(\mu^{(2)}-\mu^{(1)})}{k^{(1)}+c_1(k^{(2)}-\mu^{(1)})S_s} \tag{5}$$

166

167 where S_p ad S_s are the Eshelby tensor components:

168

169 $$S_p = \frac{\nu+1}{3(1-\nu)}\left\{1 + \frac{3}{2}\left(\frac{L^{(0)}}{R}\right)^3\left[1 - \left(\frac{R}{L^{(0)}}\right)^2 - \left(1+\frac{R}{L^{(0)}}\right)^2 e^{-\frac{2R}{L^{(0)}}}\right]\right\} \tag{6}$$

$$S_S = \frac{8-10\nu}{15(1-\nu)}\left\{1 + \frac{3}{2}\left(\frac{L^{(0)}}{R}\right)^3\left[1 - \left(\frac{R}{L^{(0)}}\right)^2 - \left(1 + \frac{R}{L^{(0)}}\right)^2 e^{-\frac{2R}{L^{(0)}}}\right]\right\} \quad (7)$$

$L^{(0)}$ and R are the material length scale parameter and the inclusion radius, respectively.

3 Results and discussion

3.1 Particle dispersion and morphology analysis

3.1.1 TGA

TGA plots of PA6-based compounds are shown in Figure 1. Due to the thermogram similarities, they are to be considered as representative of both, PA6 and PA66 compositions.

From the weight loss of the TGA curves, the percentage of polymer inside each composite in the same temperature range (c.a. 320-700°C) can be evaluated and by difference, the percentage of filler (37). The real compositions of the compounds are summarized in Table 1. Besides PA66_25, which contains 22.6 wt.% of CB, from the other compositions it can be concluded that they are close to the predicted compositions.

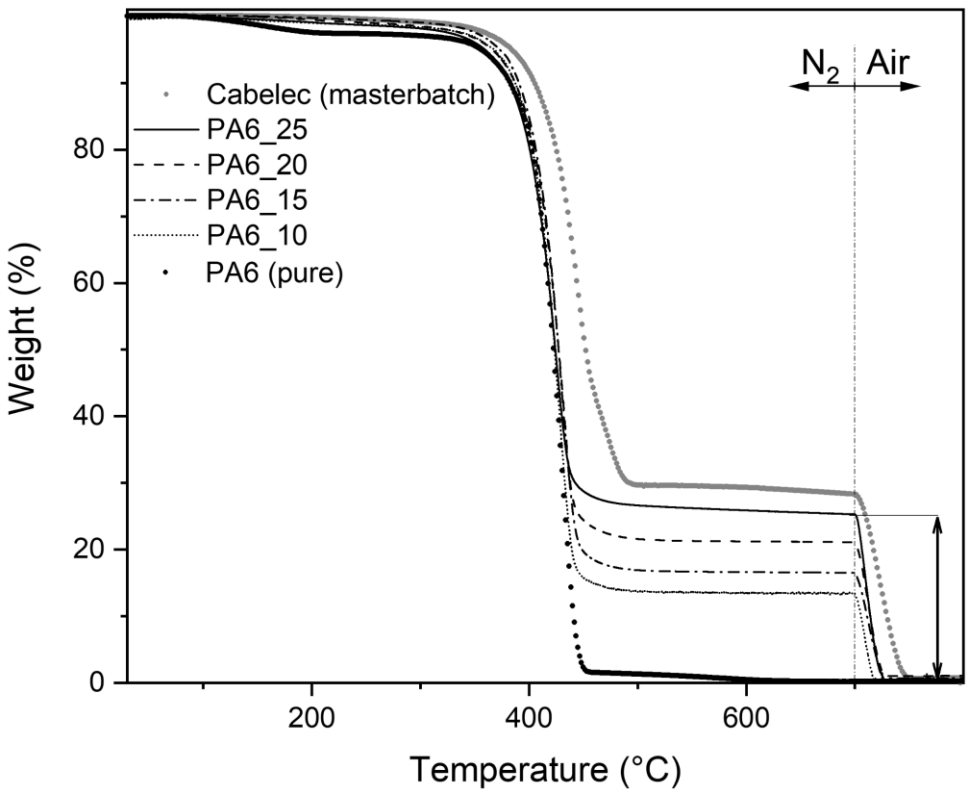

Figure 1 - TGA plots of the PA6-based compounds (gray circles: Cabelec; black solid line: PA6_25, black dashed line: PA6_20; black dotted dashed line: PA6_15; black dotted line: PA6_10, black circles: PA6, respectively) obtained under N2 (up to 700 °C) and air flow (from 700 °C up to 800 °C).

In the following sections, authors will refer to different composites by the following nomenclature: PL_wt. Where *PL* indicates the neat polymer (PA6 or PA66) and *wt* the weight percentage of carbon black (e.g., PA6_10 and PA66_10 refer to polyamide 6 and polyamide 66 loaded with CB 10 wt.%, respectively).

Table 1 - Composition of samples as obtained from TGA measurements

Label	CB (wt.%) [1]	Polymer (wt%)
Cabelec	27,5	72,5
PA6_10	12,1	87,9
PA66_10	9,7	90,5
PA6_15	15,5	84,6
PA66_15	13,7	86,3

PA6_20	19,5	80,5
PA66_20	20,0	80,0
PA6_25	23,6	76,4
PA66_25	22,6	78,4

[1] As obtained from weight loss between 800°C (air flow) and 700°C (N_2 gas flow).

3.1.2 SEM

The particle distribution was assessed for both PA6 and PA66 with the three different particle concentrations (c.a. 15%, 20% and 25% wt.). All the samples reported a uniform particle distribution. SEM images of PA6 with 25% wt. of CB are reported in Figure 2 at different magnifications: 40kX (Figure 2a), 80kX (Figure 2b) and 120kX (Figure 2c). Figures 2a, 2b and 2c are representative of the particle distribution of the whole specimen. At least 5 different zones of the specimen were analysed that reported the same distribution of the particles. Figure 2a and 2b are at lower magnification and show that the particle distribution is homogeneous and there are no areas with a lower presence of particles or agglomerates. Figure 2c shows the 120 kX magnification that highlights the particle shape and size of the carbon black particles. Figure 2c displays the presence of both spherical and elliptical shapes that are typical of CB particles. A digital image correlation software, Tescan Mira Software (Tescan, Brno, Czech Republic), has been used to study the sizes of the particles. 30 different particles were measured to assess the sizes of the elliptical and spherical shapes. The elliptical particles present an average major axis of 113 nm (±18 nm) while the minor axis is 74 nm (±15 nm). The average area of the elliptical particles is 6600 nm^2. On the other hand, the spherical particles present an average diameter of 83 nm (±16 nm) and an average area of 5400 nm^2.

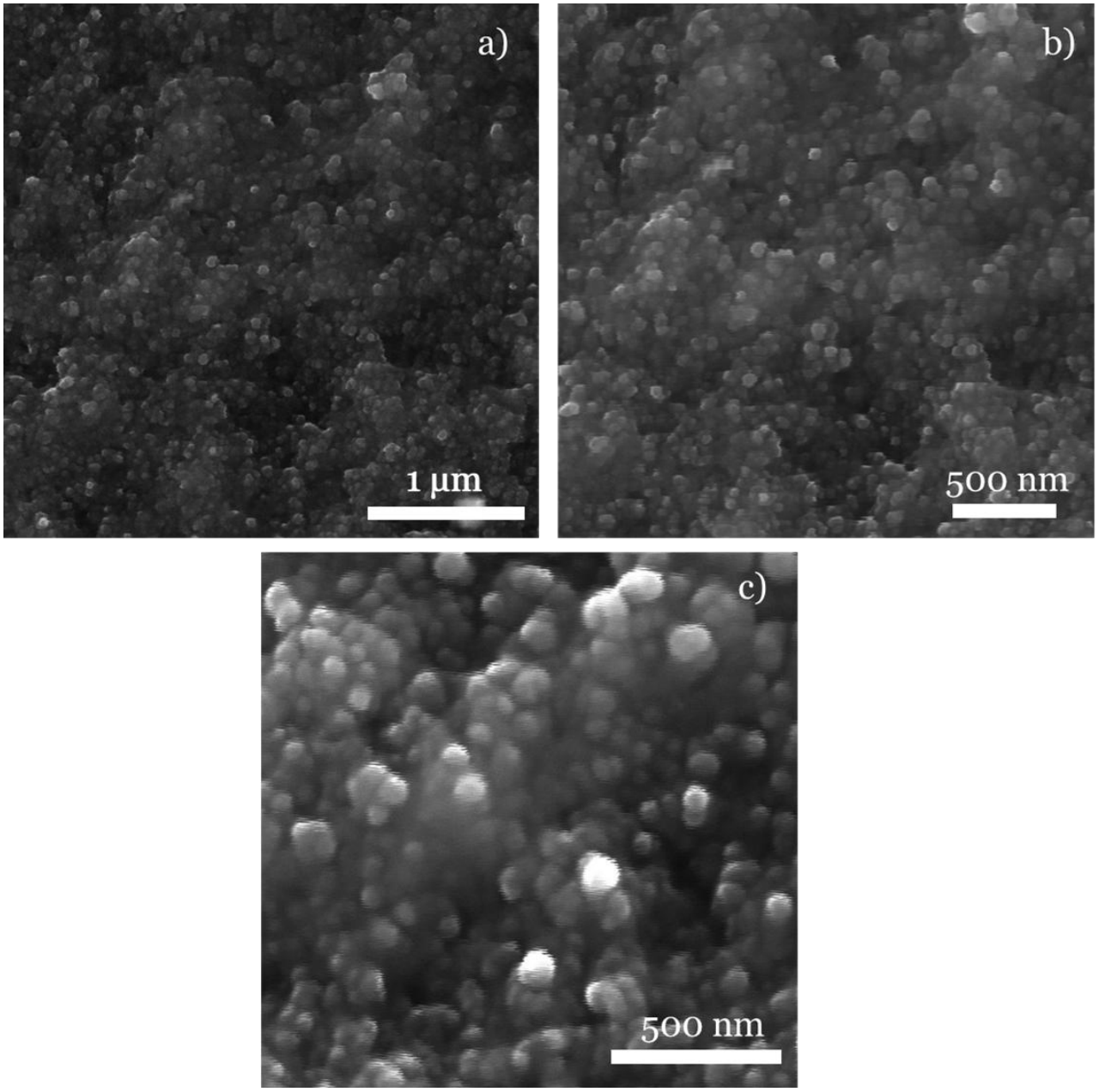

Figure 2 - SEM images of the sample PA6_25% wt. at 40 kX magnification (a), 80 kX magnification (b) and 120 kX magnification (c)Figure 3 presents SEM images of PA6_15% (3a and 3b), PA6_20% (3c and 3d) and PA6_25% (3e and 3f) at two different magnifications, 50 kX (3a, 3c and 3e) and 100 kX (3b, 3d and 3f).

The SEM images are representative of the two different materials adopted PA6 and PA66 and of the three different adopted concentrations. The lower magnifications, 3a, 3c and 3e of Figure 3 show that the particle distribution is homogeneous. The higher magnifications show that the particles are very close and there are no areas with a lower

presence of particles because all the analysed compounds are higher than the percolation point. This verification was the aim of this analysis.

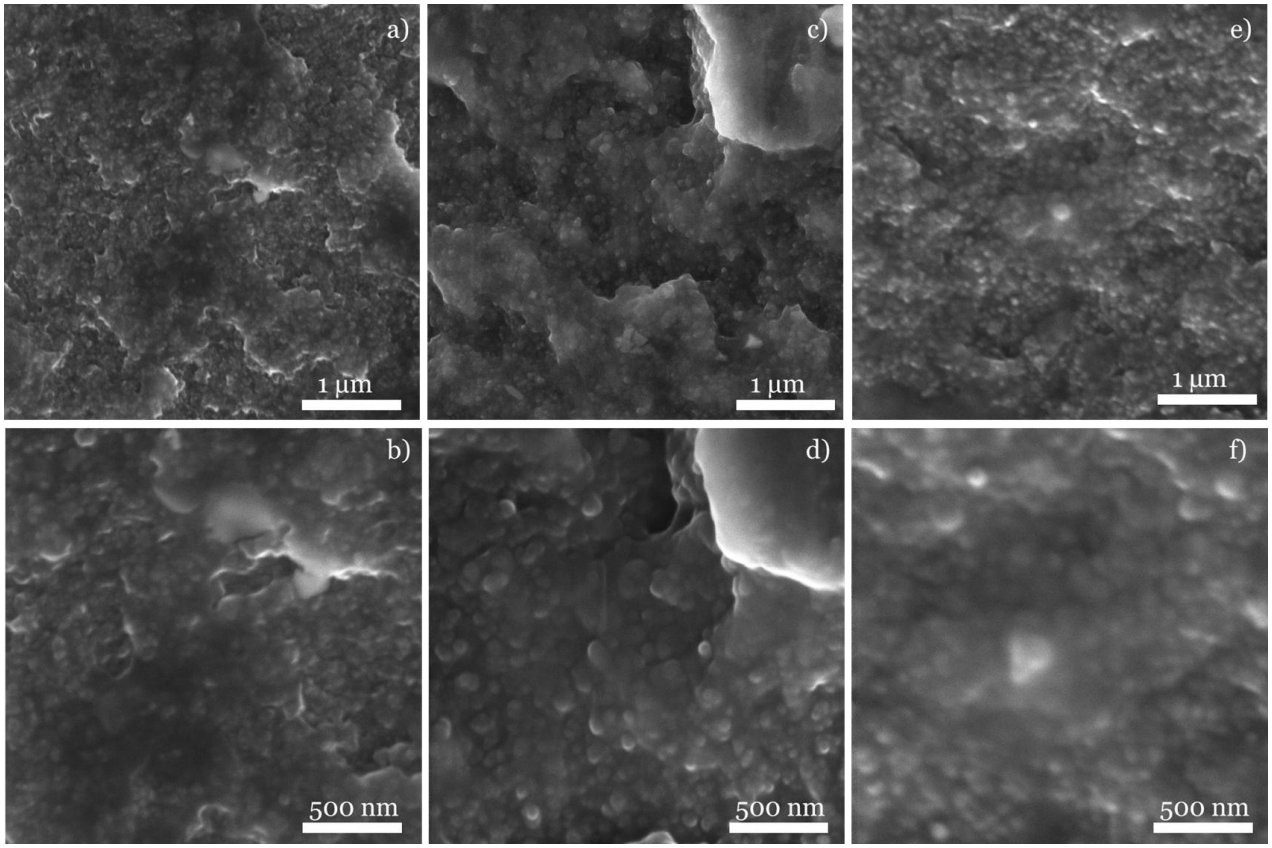

Figure 3 - SEM images at two different magnifications 50 kX (2a, 2c and 2e) and 100 kX 2b, 2d and 2f) of the samples PA6_15% (1a and 1b), PA6_20% and PA6_25%.

3.2 Percolation threshold

DC electrical resistivity of the CB-filled PA6 and PA66 composites (10-28 wt.%), measured at room temperature are shown in **Errore. L'origine riferimento non è stata trovata.**. In this figure, electrical resistivity increases with the decreasing CB loading. Notwithstanding the different injection process temperatures, the two types of

polymer composites exhibit a similar electrical behavior. Both Pa6 and PA66 based composites exhibits a resistivity increase by 7 orders of magnitude from 3,9 to 1,2×10^5 and 5,2×105 $k\Omega\, cm$, respectively.

The percolation threshold, defined as the particle concentration above which the composite goes from being a perfect insulator to a conductive, can be described by a sigmoid function in the form:

$$R = R^0 \cdot \frac{1}{1+e^{a(x-\bar{x})}} \qquad \text{(xx)}$$

Being R^0 the resistance of the insulating composite, a the coefficient describing the resistance variation with the filler loading and $\bar{x}$ the percolation threshold. Figure 4 shows the results of volumetric resistance measurements.

246

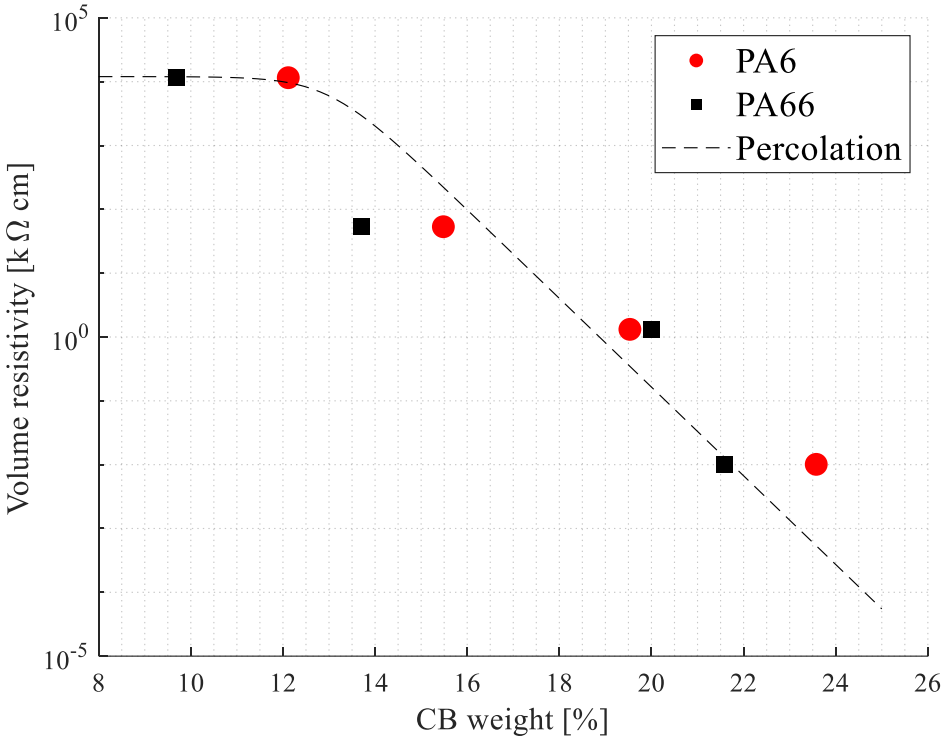
PA6
PA66
Percolation
Volume resistivity [k Ω cm]
CB weight [%]

247

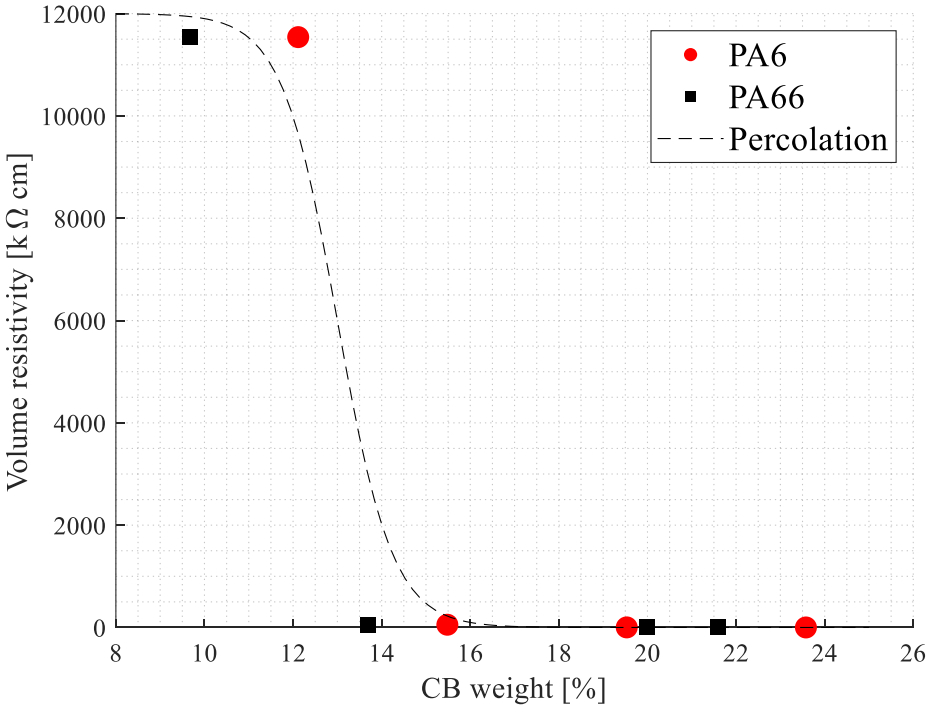
PA6
PA66
Percolation
Volume resistivity [k Ω cm]
CB weight [%]

248

Figure 4. Change in volume resistivity of CB reinforced PA6 and PA66

The sigmoid function that best approximates the resistance variation with the particle concentration has a percolation threshold of 13% with an R^0 of $12^5\ k\Omega cm$ and a coefficient α equal to 1.8.

3.3 The effect of carbon black on mechanical properties

Although the main goal of the present study is to analyze the effect of CB particles on the strain sensitivity of conductive PA/CB composites, it is fundamental to assess the composite mechanical response at first. In fact, any modification to the material composition with the goal of functionalization, should not degrade the stiffness and strength of the material itself. On the assumption of material response symmetry in tension and compression, only tensile tests are performed to evaluate the elastic modulus of composites. Experiments have been performed following the ISO D638 standards, adopting the specimen shape of type V with a minimum section of 3x3 mm and grip distance of 50 mm.

The Young Modulus and Ultimate Tensile Strength (UTS) of neat PA6 are experimentally measured as 2.4±0.1 GPa and 42±4 MPa, respectively; the bulk Young's modulus for the PA66 is found in literature as 2.5 GPa(38).

The bulk modulus of CB reinforced PA66 is monotonically increasing in the range of 10–25% weight percentage, showing a small deviation from the average value among different repetitions Figure 5 shows the measured values, the error bar and the linear trend approximating the experimental results.

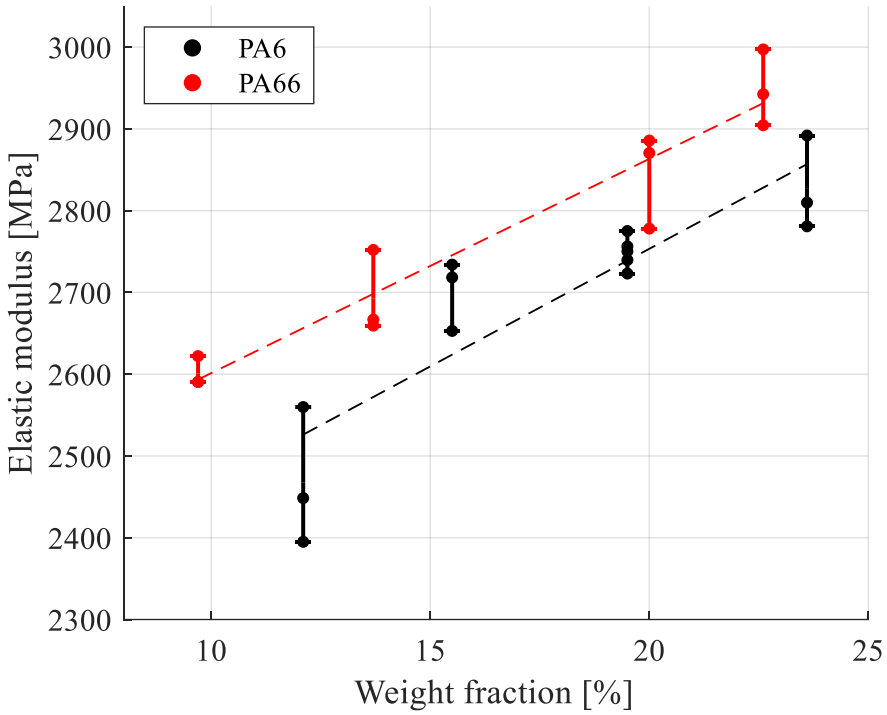

Figure 5 - Young's modulus of composites with different neat polymer and CB concentration.

Compared to the neat polymer, the bulk modulus of CB composite increases up to 20%. In PA6 composites, the particle weight percent increase from 10% to 25% lead to a 13% increase in the elastic modulus. In the case of PA66, the stiffness increases of 13% within the investigated weight percentage range. This demonstrates that the effect of the CB on the two polymers, PA6 and PA66, is consistent.

3.3.1 Mean-field homogenization models

Results from tensile tests are compared with homogenization theories described in Section 2.3. The Voigt model predicts an elastic modulus increase on average twice larger than that observed experimentally. The limit of this theory relies in the assumption of perfectly

dispersed inclusions, neglecting any interaction between particles, and any clustering carbon black spheres. Microscopies of CB morphology of the tested specimens shows a clear agglomeration formation in composite with particle weight concentration higher than 10%, yielding to the non-conformity of the Voigt hypothesis with the case under study.

As showed in Figure 6, both the Mori-Tanaka and Reuss models correctly predicts the effect of carbon black spherical inclusions on the elastic modulus increase, with a maximum error of 4% respect to the mean value. The SSGET based homogenization model is fitted with a size radius of 83 μm, as observed in SEM image in Section 2, and a material length parameter of 8.3 μm for the PA66 and 5 μm for the Nylon. Figure 6 shows that the SSGET do not correctly accounts for the particle size on the stiffening effect of CB particles for PA66 based composites. In can be concluded that the Mori-Tanaka and Reuss models can be adopted to effectively predict the elastic modulus of polyamides composites loaded with carbon black particles.

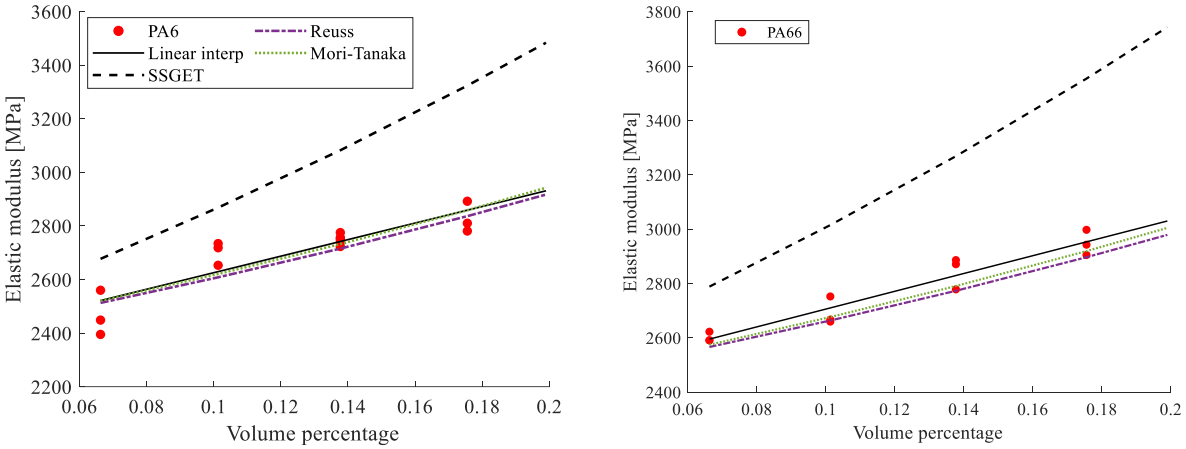

Figure 6 - Comparison of homogenization theories prediction with experimental measurements for PA6 and PA66 with different CB mass fraction

3.3.2 *Fracture surfaces (SEM)*

Figure 6 shows representative cryofractured surfaces of the PA6 (6a, 6b and 6c) and PA66 (6d, 6e, and 6f) for the three different concentrations, 15%, 20% and 25%, respectively. All the fracture surfaces are very similar and display a reproducible failure surface. There is a central area where the crack starts to propagate and appears quite smooth. Besides this area, the fracture is irregular with the presence of clear and large cracks. These two peculiar areas are more evident in Figure 6g that reports a higher magnification of the fracture surface of the specimen PA66 with 20% wt. of CB. As it is well visible in all the subfigures of Figure 6, the crack starts to propagate in the darker point of the smoother circular area. The higher magnification of Figure 6g reports the presence of one defect that was found in that area. These defects trigger the crack propagation initiation. The microscope analysis conducted on all the specimens showed that one or two defects were detected in the darker area for the two polymers prepared with the three particle concentrations. Twelve voids were measured using a digital image correlation software. These voids present a circular shape and an average diameter of 26 μm with a standard deviation of 6 μm.

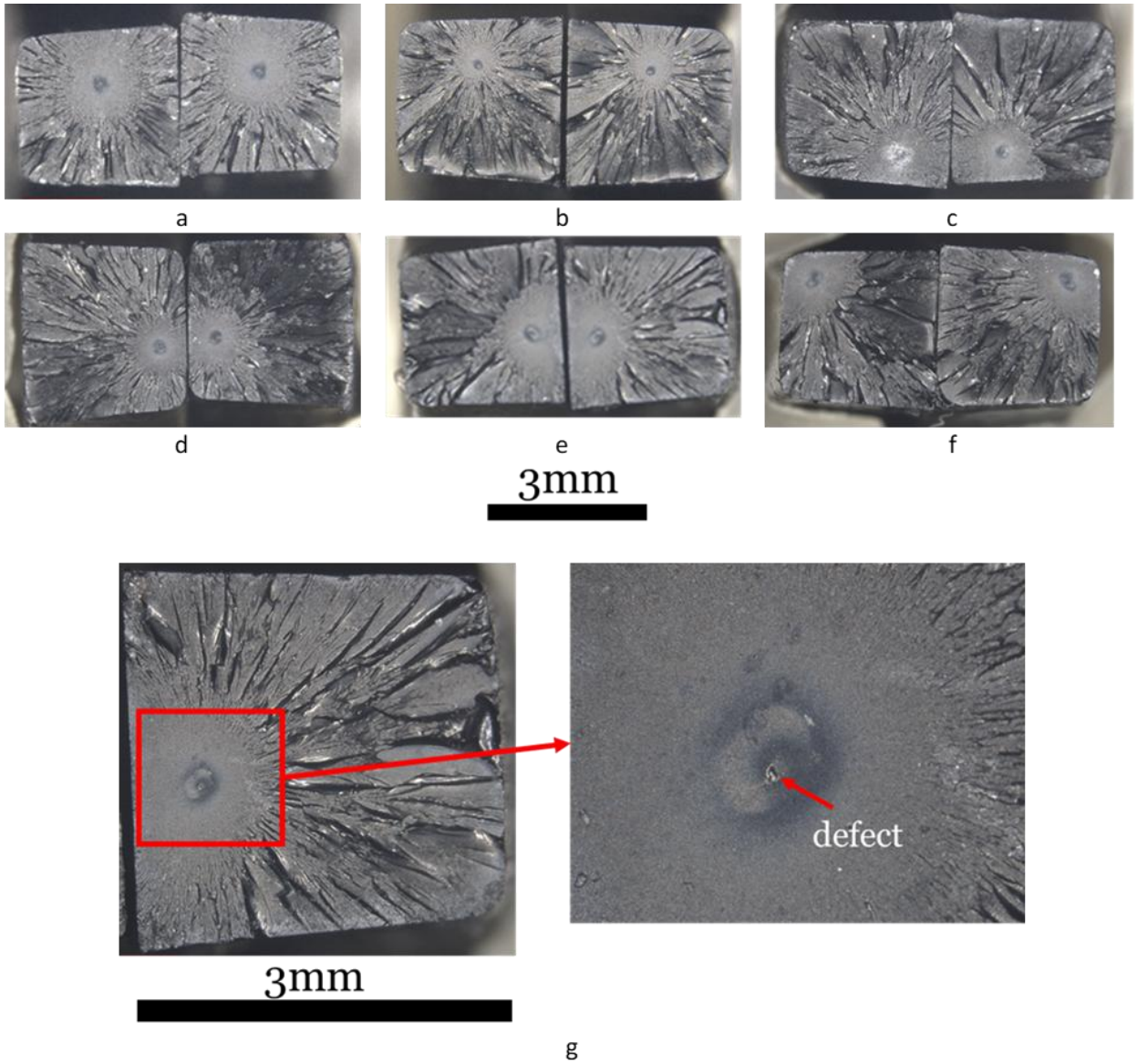

Figure 7 - Representative fracture surfaces of the PA6 and PA66 compounds

3.4 Strain sensitivity

The main goal of the present work is to study the variation of the electric passive properties induced by the mechanical strain in Carbon Black reinforced polyamides. The resistivity of composites is studied in direct current (DC) and alternate current (AC)

regime within a frequency spectrum ranging from 0 to 10 kHz. The electrical frequency response of each coupon is measured at fixed displacement increments of 0.05 mm.

From the frequency response measured at each displacement increment, it is possible to reconstruct the strain variation with respect to the applied strain for each sampled excitation frequency. First, the direct current electrical response is compared with the stress- strain curve of the material (Figure 8a) and a linear equation with null offset is fitted with the experimental measurements with a least-squares method. Figure 8b shows a comparison of the linearized strain sensitivity of dynamic impedance Z versus strain curves at three different frequencies. It is clearly highlighted the fact that strain sensitivity of the conductivity changes with the excitation frequency.

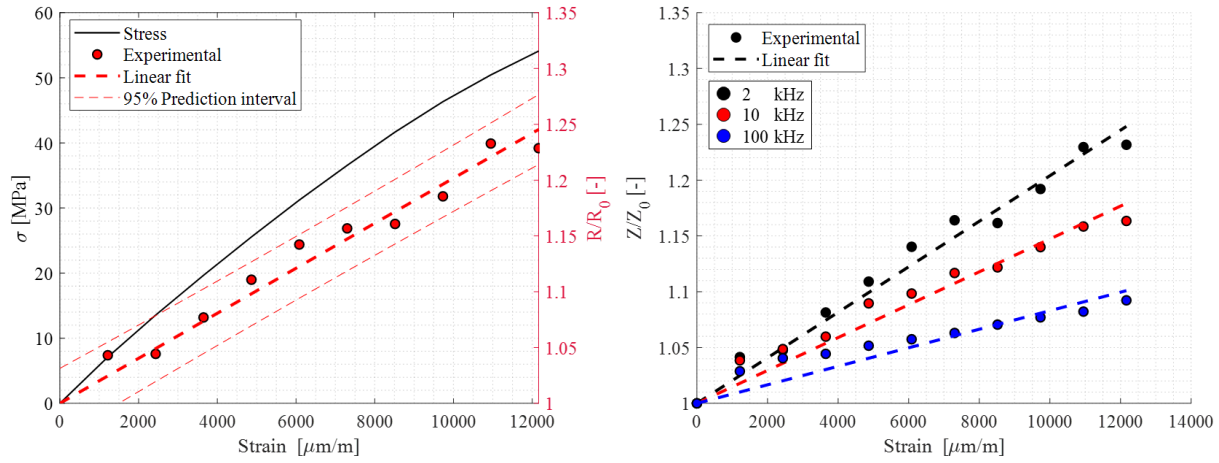

Figure 8 - a) Variation of electrical resistance compared with stress in the material, b) Variation of impedance for different frequencies. Results shown in figure are referred to PA6_20

The gauge factor GF is then computed at each excitation frequency $\bar{f}$ as:

$$GF^{\bar{f}} = \min_{G} \sum_{\varepsilon} \left(\Delta Z_{\varepsilon}^{\bar{f}} / Z_{\varepsilon=0}^{\bar{f}} - G * \varepsilon\right) \quad (8)$$

The conductivity of composites linearly varies with the logarithm of the current frequency, yielding to the equation:

$$GF = GF^{DC} + a \cdot log(f) \quad (9)$$

where a is fitted with a least-square method. Figure 9 shows the accuracy of equation 9 in predicting the dynamic gauge factor for PA6_20.

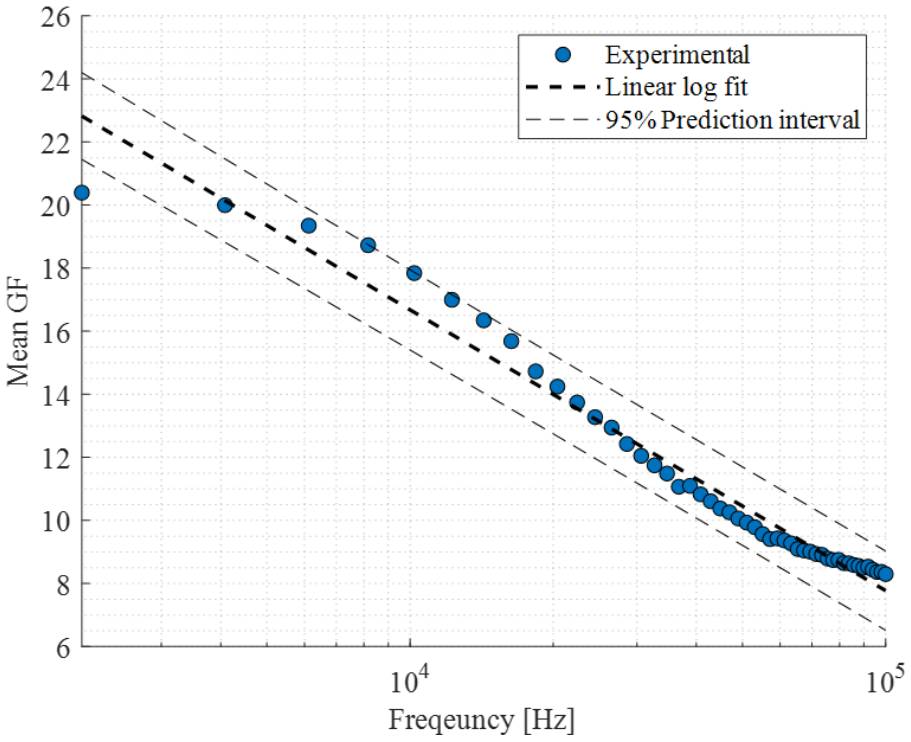

Figure 9 - Linearized Gauge Factor vs. excitation frequency for PA6_20 composite, with a=-3.9 and GF^{DC} = 23.

To assess the effect of particle concentration on the strain sensitivity, the mean GF and its standard deviation can be computed for each composite composition at each

353 excitation frequency. Eventually, the mean GF variation with excitation current
354 frequency of different composites is compared in Figure 9. Every GF measured and
355 computed across the analyzed frequency spectra, are predicted with an error lower than
356 5% by the linear logarithmic model. Figure 10 shows that there is a linear variation of the
357 dynamic gauge factor with the logarithm of excitation current frequency for each of the
358 conductive composites under study (PA66 with CB weight content of 15, 20 and 25 %).
359 Since the GF dynamic law is linear, few dynamic measures are then necessary to fit the
360 model and assess the frequency effect on the composite strain sensitivity. The slope of the
361 model goes across a sign inversion when shifting from 20% to 25% of conductive particles
362 weight content. The phenomena may be associated to the formation of inductive
363 structures of CB particles that can activate a magnetic field enhancing the current flow in
364 the composite material. This will be further investigated with experimental test for
365 concentrations between 20% and 25%, and visual analysis for the reconstruction of the
366 particles 3D arrangement at high concentrations.

367 At the best of authors knowledge, this is the first research revealing the relation
368 between the gauge factor and the alternate current excitation frequency, evidencing that
369 there is a clear influence of the AC frequency on the composite resistivity and that it is
370 different at different filler content.

371

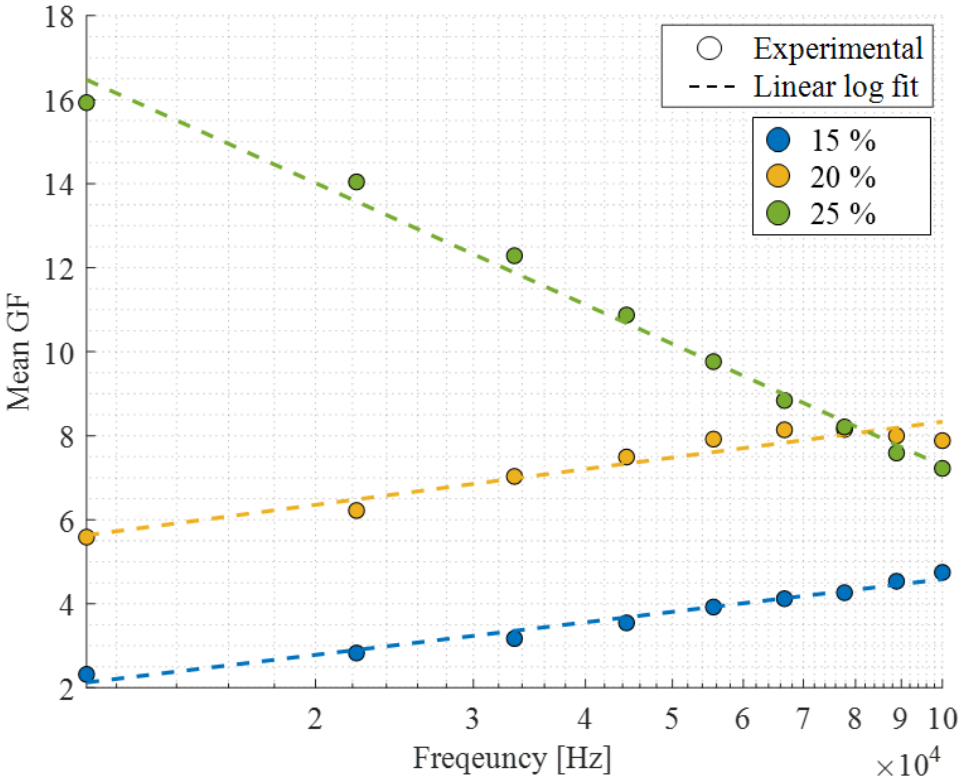

Figure 10 - Effect of carbon black particle dispersion on the strain sensitivity of PA66 in the frequency domain

Conclusions

The authors experimentally analyze the effect of carbon black on the mechanical and electrical properties of PA6 and PA66 polymers. Composite specimens are produced by injection molding, mixing the neat polymer with different weight fractions of PA6/CB compound. The evaluation of the quantity and the dispersion degree of carbon black is obtained from thermogravimetric analysis (TGA) and Field-emission Scanning Electron Microscopy (FeSEM). The effect of CB filler quantity on the elasto-plastic response is evaluated with quasi-static tensile tests and fracture surfaces are investigated with FeSEM to assess the influence of CB morphology on the composite strength. The

384 percolation threshold of different compositions has been determined by conductivity
385 measurements; conductive specimens have been tested under axial loading while in-situ
386 measuring the strain-induced change in the composite resistivity and impedance. The
387 gauge factor (GF) has been defined for different composites with different matrices at
388 different volume fractions within an electrical frequency range up to 10kHz.

389 The presented results of the experimental study demonstrated that the dispersion of
390 Carbon black particles within a PA6 and PA66 matrix enhances the stiffness and strength
391 of composite when the volume fraction is up to 20%. Nevertheless, higher concentration
392 could lead to CB agglomeration, yielding to the embrittlement of the composite. The
393 percolation threshold of polyamide/CB composite is found at 13% volume fraction of
394 carbon particles. Overall, the composite electric resistance exhibits high strain sensitivity
395 (gauge factor from 15 to 25). By analyzing the strain sensitivity of PA6 and PA66
396 composite with different Carbon Black concentration excited with different current
397 frequency, this study established that the current frequency does indeed have a
398 significant effect on the composite gauge factor, with a strong correlation to the particle
399 loading. This suggests that, while filler concentration does influence the overall
400 conductivity of the composite, the interplay of CB dispersion and excitation current
401 frequency defines the strain sensitivity of these materials. Carbon black is an ideal
402 candidate for the functionalization of fiber reinforced polyamides since it activates self-
403 sensing feature that can be enhanced by varying the current frequency, while enhancing
404 its mechanical properties. Application can be found in Structural Health Monitoring of
405 FRP parts, conductive plastic for HMI and others requiring an integrated strain sensor.

406

Acknowledgements

Authors sincerely thanks Luis Castellanos Molinas for his contribution on the set up of the experimental facilities and Alessandro Antonini for his contribution in the execution of experimental tests.

Data availability

The raw/processed data required to reproduce these findings cannot be shared at this time as the data also forms part of an ongoing study.

1. Grunlan JC, Gerberich WW, Francis LF. Electrical and mechanical behavior of carbon black-filled poly (vinyl acetate) latex-based composites. Polymer Engineering and Science. 2001 Nov;41(11):1947–62.

2. Gojny FH, Wichmann MHG, K€ Opke U, Fiedler B, Schulte K. Carbon nanotube-reinforced epoxy-composites: enhanced stiffness and fracture toughness at low nanotube content. 2004; Available from: www.elsevier.com/locate/compscitech

3. Phong NT, Gabr MH, Okubo K, Chuong B, Fujii T. Improvement in the mechanical performances of carbon fiber/epoxy composite with addition of nano- (Polyvinyl alcohol) fibers. 2013; Available from: http://dx.doi.org/10.1016/j.compstruct.2012.12.018

4. Ciardiello R, Drzal LT, Belingardi G. Effects of carbon black and graphene nano-platelet fillers on the mechanical properties of syntactic foam. 2017; Available from: http://dx.doi.org/10.1016/j.compstruct.2017.07.057

5. Lee G, Sung M, Ho Youk J, Lee J, Yu WR. Improved tensile strength of carbon nanotube-grafted carbon fiber reinforced composites. 2019; Available from: https://doi.org/10.1016/j.compstruct.2019.04.037

6. Cochrane C, Koncar V, Lewandowski M, Dufour C. Design and Development of a Flexible Strain Sensor for Textile Structures Based on a Conductive Polymer Composite. Sensors [Internet]. 2007;7:473–92. Available from: www.mdpi.org/sensors

7. Heiser JA, King JA, Konell JP, Miskioglu I, Sutter LL. Tensile and impact properties of carbon filled Nylon-6,6 based resins. Journal of Applied Polymer

438 Science. 2004 Mar 5;91(5):2881–93.

439 8. Wang J, Ma C, Chen G, Dai P. Interlaminar fracture toughness and conductivity of
440 carbon fiber/epoxy resin composite laminate modified by carbon black-loaded
441 polypropylene non-woven fabric interleaves. 2019; Available from:
442 https://doi.org/10.1016/j.compstruct.2019.111649

443 9. Cesano F, Uddin MJ, Damin A, Scarano D. Multifunctional Conductive Paths
444 Obtained by Laser Processing of Non-Conductive Carbon Nanotube/Polypropylene
445 Composites. 2021; Available from: https://doi.org/10.3390/nano11030604

446 10. Cravanzola S, Haznedar G, Scarano D, Zecchina A, Cesano F. Carbon-based
447 piezoresistive polymer composites: Structure and electrical properties. 2013;
448 Available from: http://dx.doi.org/10.1016/j.carbon.2013.05.064

449 11. Zhang Q, Wang J, Zhang BY, Guo BH, Yu J, Guo ZX. Improved electrical
450 conductivity of polymer/carbon black composites by simultaneous dispersion and
451 interaction-induced network assembly. Composites Science and Technology. 2019
452 Jul 28;179:106–14.

453 12. Zhao J, Dai K, Liu C, Zheng G, Wang B, Liu C, et al. A comparison between strain
454 sensing behaviors of carbon black/polypropylene and carbon
455 nanotubes/polypropylene electrically conductive composites. Composites Part A:
456 Applied Science and Manufacturing [Internet]. 2013;48(1):129–36. Available from:
457 http://dx.doi.org/10.1016/j.compositesa.2013.01.004

458 13. Mahmood H, Vanzetti L, Bersani M, Pegoretti A. Mechanical properties and strain
459 monitoring of glass-epoxy composites with graphene-coated fibers. Composites

460 Part A: Applied Science and Manufacturing. 2018;107:112–23.

461 14. Spinelli G, Lamberti P, Tucci V, Vertuccio L, Guadagno L. Experimental and
462 theoretical study on piezoresistive properties of a structural resin reinforced with
463 carbon nanotubes for strain sensing and damage monitoring. Composites Part B:
464 Engineering [Internet]. 2018;145(March):90–9. Available from:
465 https://doi.org/10.1016/j.compositesb.2018.03.025

466 15. Moriche R, Sánchez M, Prolongo SG, Jiménez-Suárez A, Ureña A. Reversible
467 phenomena and failure localization in self-monitoring GNP/epoxy
468 nanocomposites. Composite Structures. 2016;136:101–5.

469 16. Moriche R, Sánchez M, Jiménez-Suárez A, Prolongo SG, Ureña A. Strain
470 monitoring mechanisms of sensors based on the addition of graphene
471 nanoplatelets into an epoxy matrix. Composites Science and Technology.
472 2016;123:65–70.

473 17. Koecher MC, Pande JH, Merkley S, Henderson S, Fullwood DT, Bowden AE.
474 Piezoresistive in-situ strain sensing of composite laminate structures. Composites
475 Part B: Engineering [Internet]. 2015;69:534–41. Available from:
476 http://dx.doi.org/10.1016/j.compositesb.2014.09.029

477 18. Kumar S, Falzon BG, Hawkins SC. Ultrasensitive Embedded Sensor for Composite
478 Joints Based on a Highly Aligned Carbon Nanotube Web. Carbon N Y [Internet].
479 2019;149:380–9. Available from: https://doi.org/10.1016/j.carbon.2019.04.044

480 19. Cai JH, Li J, Chen XD, Wang M. Multifunctional polydimethylsiloxane foam with
481 multi-walled carbon nanotube and thermo-expandable microsphere for

temperature sensing, microwave shielding and piezoresistive sensor. Chemical Engineering Journal. 2020 Aug 1;393:124805.

20. Chen YF, Huang ML, Cai JH, Weng YX, Wang M. Piezoresistive anisotropy in conductive silicon rubber/multi-walled carbon nanotube/nickel particle composites via alignment of nickel particles. Composites Science and Technology. 2022 Jul 7;225:109520.

21. Chen YF, Li J, Tan YJ, Cai JH, Tang XH, Liu JH, et al. Achieving highly electrical conductivity and piezoresistive sensitivity in polydimethylsiloxane/multi-walled carbon nanotube composites via the incorporation of silicon dioxide micro-particles. Composites Science and Technology. 2019 Jun 16;177:41–8.

22. Zhan P, Zhai W, Wang N, Wei X, Zheng G, Dai K, et al. Electrically conductive carbon black/electrospun polyamide 6/poly(vinyl alcohol) composite based strain sensor with ultrahigh sensitivity and favorable repeatability. Materials Letters. 2019 Feb 1;236:60–3.

23. Qu Y, Xu P, Liu H, Li Q, Wang N, Zhao S, et al. Tunable temperature-resistivity behaviors of carbon black/polyamide 6 /high-density polyethylene composites with conductive electrospun PA6 fibrous network.

24. Vertuccio L, Guadagno L, Spinelli G, Lamberti P, Tucci V, Russo S. Piezoresistive properties of resin reinforced with carbon nanotubes for health-monitoring of aircraft primary structures. Composites Part B: Engineering [Internet]. 2016;107:192–202. Available from: http://dx.doi.org/10.1016/j.compositesb.2016.09.061

25. Chen CK, Kuo JK. Nylon 6/CB polymeric conductive plastic bipolar plates for PEM fuel cells. Journal of Applied Polymer Science. 2006 Sep 5;101(5):3415–21.

26. Lim JW, Kim M, Ho Y, Dai Y, Lee G. Development of carbon/PEEK composite bipolar plates with nano-conductive particles for High-Temperature PEM fuel cells (HT-PEMFCs). 2014; Available from: http://dx.doi.org/10.1016/j.compstruct.2014.08.011

27. Müller MT, Pötzsch HF, Gohs U, Heinrich G. Online structural-health monitoring of glass fiber-reinforced thermoplastics using different carbon allotropes in the interphase. Materials. 2018;11(7).

28. Sam-Daliri O, Farahani M, Faller LM, Zangl H. Structural health monitoring of defective single lap adhesive joints using graphene nanoplatelets. Journal of Manufacturing Processes. 2020;55(March):119–30.

29. Chiacchiarelli LM, Rallini M, Monti M, Puglia D, Kenny JM, Torre L. The role of irreversible and reversible phenomena in the piezoresistive behavior of graphene epoxy nanocomposites applied to structural health monitoring. Composites Science and Technology [Internet]. 2013;80:73–9. Available from: http://dx.doi.org/10.1016/j.compscitech.2013.03.009

30. Zhang H, Bilotti E, Peijs T. The use of carbon nanotubes for damage sensing and structural health monitoring in laminated composites: a review. Nanocomposites [Internet]. 2015;1(4):167–84. Available from: http://dx.doi.org/10.1080/20550324.2015.1113639

31. Nanni F, Ruscito G, Puglia D, Terenzi A, Kenny JM, Gusmano G. Effect of carbon

526 black nanoparticle intrinsic properties on the self-monitoring performance of glass
527 fibre reinforced composite rods. Composites Science and Technology. 2011 Jan
528 1;71(1):1–8.

529 32. Voigt W. Ueber die Beziehung zwischen den beiden Elasticitätsconstanten
530 isotroper Körper. Ann Phys [Internet]. 1889 Jan 1 [cited 2022 Feb
531 10];274(12):573–87. Available from:
532 https://onlinelibrary.wiley.com/doi/full/10.1002/andp.18892741206

533 33. Willis JR. Variational and Related Methods for the Overall Properties of
534 Composites. Advances in Applied Mechanics. 1981 Jan 1;21(C):1–78.

535 34. Morit T, Tanaka7 $ K. AVERAGE STRESS IN MATRIX AND AVERAGE ELASTIC
536 ENERGY OF MATERIALS WITH MISFITTING INCLUSIONS*.

537 35. Hill RR. A SELF-CONSISTENT MECHANICS OF COMPOSITE MATERIALS. Vol.
538 13, 1. Mech. Phys. Solids. Pergamon Press Ltd. Printed in Cleat Britain; 1965.

539 36. Ma HM, Gao XL. A new homogenization method based on a simplified strain
540 gradient elasticity theory. Acta Mech. 2014;225:1075–91.

541 37. Brunella V, Rossatto BG, Scarano D, Cesano F. Thermal, Morphological, Electrical
542 Properties and Touch-Sensor Application of Conductive Carbon Black-Filled
543 Polyamide Composites. 2021; Available from:
544 https://doi.org/10.3390/nano11113103

545 38. Pé Ron M, Dé Ric Jacquemin F, Casari P, Orange G, Bailleul JL, Boyard N.
546 Thermomechanical characterization of a low viscosity PA66 thermoplastic
547 matrix and associated continuous glass fibre composite under processing